Secondary electron emission yield from high aspect ratio carbon velvet surfaces

Chenggang Jin, Angelica Ottaviano, and Yevgeny Raitses

Citation: Journal of Applied Physics **122**, 173301 (2017);
View online: https://doi.org/10.1063/1.4993979
View Table of Contents: http://aip.scitation.org/toc/jap/122/17
Published by the American Institute of Physics

Secondary electron emission yield from high aspect ratio carbon velvet surfaces

Chenggang Jin,[a] Angelica Ottaviano, and Yevgeny Raitses[b]
Princeton Plasma Physics Laboratory, Princeton, New Jersey 08543, USA

(Received 3 July 2017; accepted 12 October 2017; published online 1 November 2017)

The plasma electrons bombarding a plasma-facing wall surface can induce secondary electron emission (SEE) from the wall. A strong SEE can enhance the power losses by reducing the wall sheath potential and thereby increasing the electron flux from the plasma to the wall. The use of the materials with surface roughness and the engineered materials with surface architecture is known to reduce the effective SEE by trapping the secondary electrons. In this work, we demonstrate a 65% reduction of SEE yield using a velvet material consisting of high aspect ratio carbon fibers. The measurements of SEE yield for different velvet samples using the electron beam in vacuum demonstrate the dependence of the SEE yield on the fiber length and the packing density, which is strongly affected by the alignment of long velvet fibers with respect to the electron beam impinging on the velvet sample. The results of SEE measurements support the previous observations of the reduced SEE measured in Hall thrusters. *Published by AIP Publishing.* https://doi.org/10.1063/1.4993979

I. INTRODUCTION

The plasma-wall interaction in the presence of a strong secondary electron emission (SEE) is relevant to various plasma applications, including but not limited to electric propulsion,[1,2] magnetic fusion devices,[3,4] and plasma processing devices.[5,6] The plasma electrons bombarding the plasma-facing wall surface can be scattered back to the plasma (backscattering SEE) or induce the ejection of the secondary electrons from the material (true SEE). Independent on the nature of secondary electrons, a strong SEE can enhance power losses from the plasma due to the reduction of the plasma-wall sheath potential.[7] These losses increase with the increase of the total SEE yield, which is defined as the ratio of the total emitted electron flux, including true and backscattered electrons, to the incident electron flux. When the SEE yield approaches 1, the sheath may enter the so-called space-charge limited regime[8] or the inverse sheath regime.[9] Under such conditions, the wall acts as a very effective heat sink for the plasma. The suppression of SEE would be beneficial for many plasma applications[1–6] in which the wall losses can cause a degradation of performance of plasma devices or overheating of the plasma-facing walls.

There are different ways to reduce and even suppress the SEE yield. In Ref. 10, a surface treatment by different processes, including electropolishing, carbon coating, and vacuum pyrolyzing was shown to reduce the SEE yield by 28% compared to the untreated surfaces of the same materials. Another approach to the suppression of SEE uses complex structured surfaces, which trap the SEE electrons. For example, coating of the aluminum surface with nanostructured graphene platelets allowed a 60% reduction of the total SEE yield as compared to the uncoated aluminum surface.[11] In Ref. 12, copper oxide nanowires grown on copper were used to mitigate the effect of SEE in radio frequency (RF) amplifiers. Moreover, Cu foams were shown to allow a drastic (50%) reduction of the SEE yield.[13] These foams were proposed for application in particle accelerators. In Ref. 14, it was demonstrated that the SEE yield from the tungsten fuzz produced in a helium gas discharge, decreases significantly compared to the smooth tungsten surface. Finally, the experimental and theoretical studies of Ref. 15 investigated the SEE yield from a micro-porous metal array, and demonstrated a strong dependence of the SEE yield on the micropore geometry and a number of micro-pores per unit area of the array. They predicted and demonstrated a 45% reduction of the SEE yield as compared to the Ag surface for an optimized array.

Unlike a majority of the previous studies of SEE yield from the architecture surfaces with low aspect ratio surface non-uniformities (e.g., roughened surface) ($A_R \equiv h/r < 10^2$, where A_R is the aspect ratio of a surface non-uniformity, h and r are the characteristic length and diameter of this non-uniformity, respectively), this work is aimed to characterize the SEE yield from high aspect ratio ($A_R > 10^3$) velvet surfaces. A carbon velvet material was already successfully used for the suppression of SEE in Hall thrusters.[16] A typical velvet material consists of fully or partially aligned fibers attached to a substrate. In Ref. 17, the SEE yield from the velvet surface was investigated numerically and analytically. The obtained analytical solution and simulations confirmed the hypothesis of Ref. 15 that the total SEE yield of the velvet can be significantly smaller than the SEE yield for a planar surface and even for a roughened surface with a micro-porous array. The reduction of SEE yield comes from the fact that SEE electrons produced deep inside the velvet have a large probability of hitting a fiber and getting absorbed by the surface before exiting the velvet. Such trapped secondary electrons do not contribute to the flux of secondary electrons from the surface to the plasma. Thus, undesired effects of

[a]Permanent address: College of Physics, Optoelectronics and Energy, and Collaborative Innovation Center of Suzhou Nano Science and Technology, Soochow University, Suzhou 215006, China.
[b]Author to whom correspondence should be addressed: yraitses@pppl.gov

SEE on the plasma can be greatly suppressed. In this paper, the total SEE yield from various carbon velvet surfaces was directly measured in vacuum using an electron beam. In particular, it is shown that the SEE yield depends on the velvet characteristics, including the fiber length and the fiber packing density, and the angle of incidence of the primary electrons with respect to the velvet substrate.

II. VELVET SAMPLES AND EXPERIMENTAL SETUP

A. Determination of the actual packing density of velvet samples

The total SEE yield was characterized for five different carbon velvet samples with different packing densities and fiber lengths (Table I), as well as planar graphite substrates without velvet. The velvet samples are composed of cylindrical carbon fibers of radius $\sim 3.5\,\mu$m attached to a planar graphite surface of a 25 mm-diameter substrate. For an ideal velvet sample with velvet fibers aligned normal to the substrate surface, the designed (or manufacturer specified) packing density is defined as the ratio of the total area of all the fiber tips attached to the sample substrate to the total area of this sample. For example, 3.0% of packing density indicates that 3.0% of the sample is occupied by fiber tips when viewed from above. However, a microscopic analysis of the velvet samples used in these experiments revealed that for all these samples, there are misaligned velvet fibers bended with respect to the planar substrate surface of the samples. For example, Fig. 1 shows images of a velvet sample obtained with an FEI Quanta 200 FEG Environmental Scanning Electron Microscope (SEM). The images were obtained by irradiation of the velvet sample with the SEM electron beam of 15 keV at normal incidence to the sample. It can be clearly seen that the fiber areas that are visible in SEM micrographs include portions of the side surface of the fibers as well as the fiber tips. This is because the primary electrons of the SEM electron beam impinge these side walls producing SEE electrons detected by a SEM detector.

It is reasonable to assume that in practical plasma applications of such velvet materials, the primary electrons directed normal to the substrate surface would also hit the side walls of the bended fibers. Therefore, from the standpoint of suppression of SEE by the trapping of secondary electrons, the actual packing density is apparently different from the designed packing density. Table I describes the geometrical characteristics of the velvet samples including the fiber lengths, and the designed and actual packing densities.

TABLE I. Properties of velvet samples used in the described experiments.

Sample	Fiber length (mm)	Designed packing density (%)	Aspect ratio (height/radius)	Actual packing density (%)	Error (%)
1	0.5	4	145	85	2.3
2	1.5	3.5	430	81	5.8
3	1.5	1.8	430	68	5
4	1.5	0.8	430	63	2.8
5	3	2.7	860	87	4.7

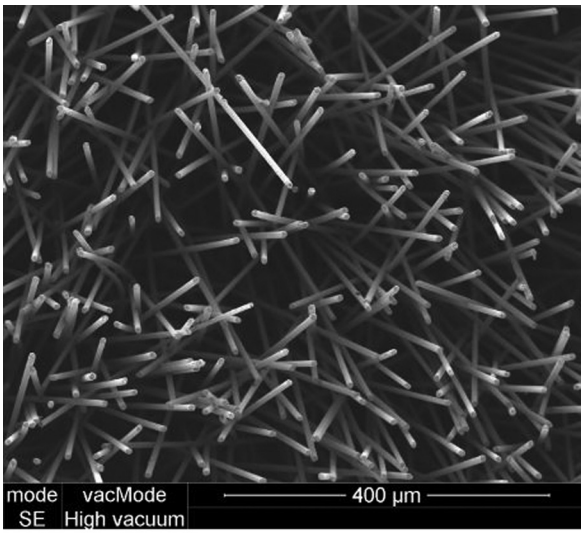

(a)

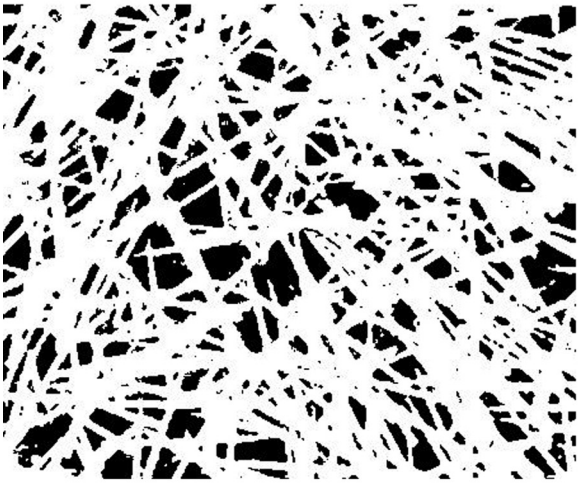

(b)

FIG. 1. (a) An SEM micrograph of carbon velvet with 1.5 mm fiber length and the designed packing density (as specified by a manufacturer) 1.8%, (b) the same SEM micrograph post-processed by thresholding the pixels of velvet images. The actual packing density estimated using Eq. (1) is 69.5%.

The actual packing density, A, was determined by post-processing of several SEM micrographs for each carbon velvet sample. The parameters of SEM, such as image contrast, brightness, and beam spot size were kept constant for all the velvet samples. The image processing consists of separating all the pixels of the velvet images into fiber pixels and graphite base pixels. This was achieved by thresholding the SEM images at the average intensity of the graphite base pixels. The actual packing density was then estimated as the ratio of number of fiber pixels, n_f, to the total number of pixels in an image with horizontal and vertical pixel dimensions n and m, respectively

$$A = \frac{n_f}{n \times m}. \tag{1}$$

Here, n_f is defined as the number of pixels, which have an intensity larger than the graphite base pixel intensity. Figure 1(b) shows the post-processed SEM micrograph using Eq. (1).

The error in the last column of Table I is the percent deviation from the average actual packing density using 10 velvet images for each sample. The uncertainty varies between the samples due to non-uniformity in fiber orientation across the surface of a single velvet sample. In the same sample, there is a large spread in the angles of the velvet fibers, leading to high error margins when averaging over all the real packing densities of the sample. This feature is easily observed by surveying the velvet surfaces using SEM.

B. Measurements of the total SEE yield

The measurements of the total SEE yield from the velvet and graphite samples were conducted in an ultra-high vacuum chamber (base pressure at $1-5\times10^{-8}$ Torr) using an experimental setup similar to Ref. 18. A Kimball Physics ELG-2 electron gun produced primary electrons with energies of 6–1000 eV. Throughout all the experiments described in this paper, the maximum electron beam current did not exceed 2 mA. For measurements, each sample was exposed to the electron beam from the gun. In addition, in order to shield the exposed sample from stray electric fields an aluminum collector was attached to the gun and placed above the sample axisymmetrically with both the gun and the sample. The collector was electrically insulated from the gun and the sample in order to allow for changes of the collector bias voltage with respect to the sample and the gun.

In experiments, the samples were exposed normal to the beam and at 90° to the beam (Fig. 2). A Keithley 6485 picoammeter was used to measure the current in the sample circuit and the collector circuit (Fig. 3). The electron beam from the gun was first characterized using a Faraday cup with an entrance opening of 3 mm-diameter to ensure that the beam is centered on the sample. The primary electron current, I_{PE}, was measured on the sample biased to +18 V with respect to ground, while the collector was electrically connected to

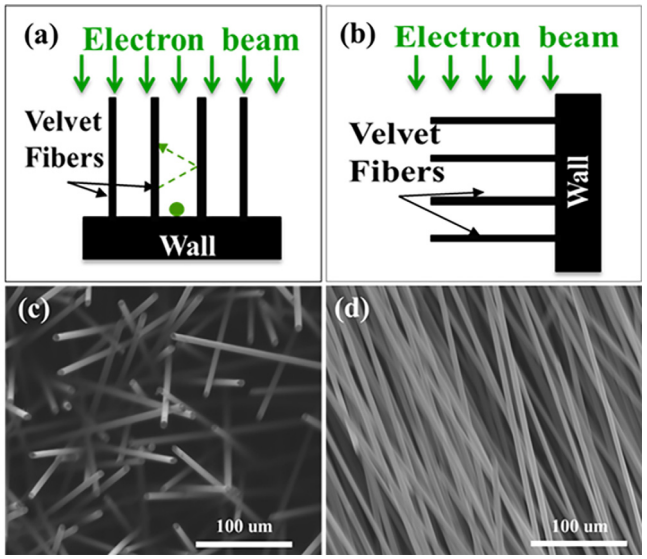

FIG. 2. Schematics of the velvet sample with fibers (a) parallel to the primary electron beam, (b) perpendicular to the primary electron beam, and the corresponding SEM micrographs of the velvet: (c) top view and (d) side view.

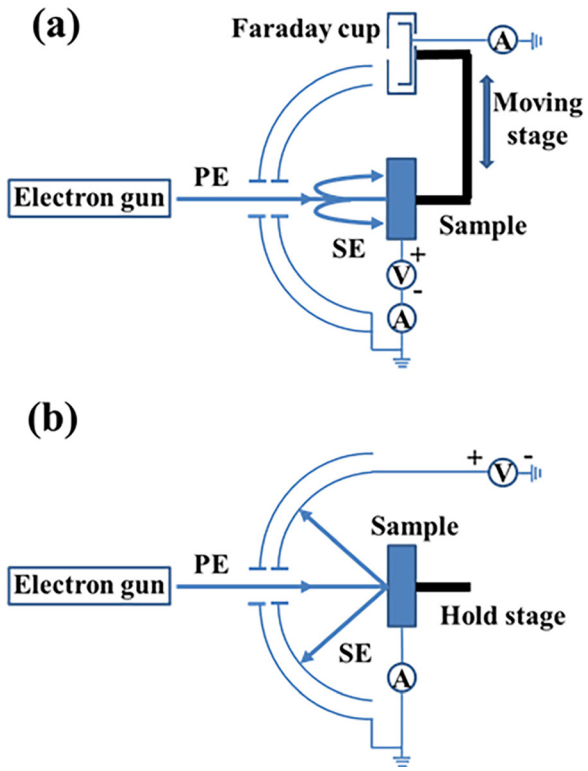

FIG. 3. Experimental setup for measurements of the SEE yield: (a) measurements of the primary electron current, and (b) measurements of the sample current.

the ground. A positive bias voltage of the sample ensured both the collection of beam electrons by the sample circuit and the suppression of secondary electrons from the sample. The sample current $I_S = I_{PE} - I_{SE}$, which includes contributions from both secondary electrons, I_{SE}, and the primary electrons, was measured on the sample connected electrically to the ground through the picoammeter. In these measurements, the collector was biased +18 V with respect to grounded sample to prevent the collection of tertiary electrons from the grounded chamber wall. Then, the total SEE yield was deduced from

$$\gamma_e = \frac{I_{SE}}{I_{PE}} = \frac{I_{PE} - I_S}{I_{PE}} = 1 - \frac{I_S}{I_{PE}}. \quad (2)$$

For each velvet sample, the total SEE yield was measured at normal and 45° incidence to the sample surface.

III. RESULTS AND DISCUSSIONS

Figure 4 compares the total SEE yield from velvet samples 2, 3, and 4 with the same fiber length of 1.5 mm and the total SEE yield from two planar graphite samples, including a graphite sample from Ref. 19, and a graphite substrate used for the velvet samples, but without velvet fibers. For all these samples, the SEE yield reaches its maximum at ~300 eV. For the velvet samples, the SEE yield is lower than the SEE yield from the planar graphite samples. This result supports the hypothesis of the trapping of secondary electrons in velvet fibers proposed in Ref. 16 and generally consistent with the predictions of Ref. 17. For the samples with the same fiber length, the sample with the largest packing density (sample 2)

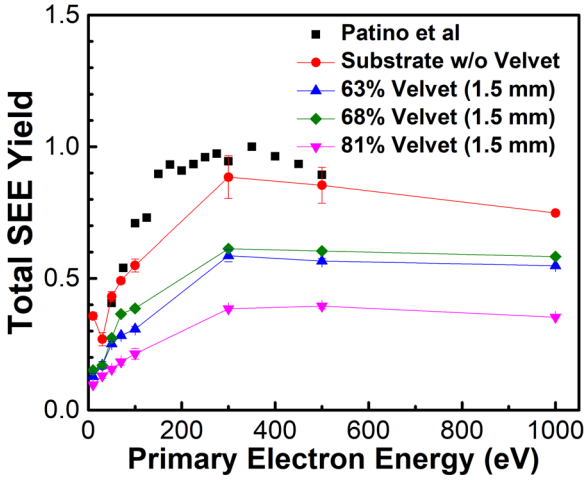

FIG. 4. The total SEE yield from carbon velvet samples with a fiber length of 1.5 mm and different values of the actual packing density (63%–81%) as a function of the electron energy of primary electrons from the electron gun. For comparison, the SEE yield for graphite substrate without velvet (red filled circles) and Ref. 19 (black filled squares) are also plotted.

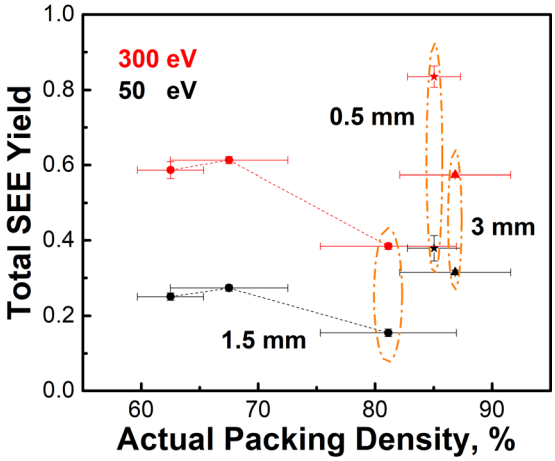

FIG. 5. The effect of the actual packing density on total SEE yield for the velvet samples with different fiber lengths: 0.5 mm (pentagon-shape symbols), 1.5 mm (circle-shape symbols), and 3 mm (triangle-shape symbols). The measurements are shown for two energies of primary electrons: 50 eV (black symbols) and 300 eV (red symbols).

has the lowest SEE yield (Fig. 4). The velvet samples display a decreasing trend in the SEE yield with an increase of the actual packing density from 63% to 81%. This trend does not seem to hold for samples 3 and 4 with the actual packing densities of 68% and 63%, respectively. The SEE yield of sample 4 is somewhat smaller than the SEE yield of sample 3. This deviation from the trend is attributed to the errors in the actual packing densities for sample 3 (5%) and sample 4 (2.8%). Reference 17 predicted the existence of optimal packing density for a given fiber aspect ratio. This optimum packing density was predicted due to a tradeoff between contributions of the fiber tips and the side walls to the SEE from the velvet. It is possible that in our set of velvet samples with the same fiber aspect ratio, there are no samples with such optimal packing density or the packing density larger than this optimal value.

It is interesting that for the samples with the closest packing densities (samples 1, 2 and 5 $\sim$ 81%–87%), the samples with the shortest and longest fibers (samples 1 and 5) have the larger yield than sample 2 with the fiber length of 1.5 mm. This result, which seemingly indicates the existence of the optimal fiber length, is not consistent with the predictions of Ref. 17 and is shown in Fig. 5. The model predicts the reduction of the SEE yield with the fiber length probably up to the saturation of the SEE yield above the certain fiber length (aspect ratio) when the contribution of the SEE electrons from the bottom of the velvet substrate becomes negligible as compared to the contribution from the fiber tops and sides. This unexpected result is likely due to the bending of the longer fibers [Figs. 1(a) and 2(c)] of sample 5. Such bended fibers are tilted away from the normal incidence of the primary electron beam from the gun. Since the SEE yield is affected by the incidence angle,[20] the bended fibers have larger SEE yield than the fibers aligned with the beam. The bended fibers were not considered on the models and simulations of Ref. 17 that may explain the earlier contradiction between experiment and modeling.

To explore the effect of the incidence angle of primary electrons on SEE, we conducted measurements of the total SEE yield for both the normal incidence and the oblique incidence. Figure 6 compares the total SEE yield from the velvet sample 2 and the planar graphite substrate without velvet. The SEE yield form substrate follows a $1/\cos(\theta)$ dependence (i.e., $\gamma_0(45^\circ) = \gamma_0(0^\circ)/\cos(45^\circ)$, where γ_0 is the SEE yield at the normal incidence). The increase of SEE yield at grazing angles is due to the increased generation of the secondary electrons within the material escape depth.[21] Apparently, for the velvet sample, the angular dependence does not follow the cosine law. In particular, the yield at oblique incidence is generally larger than it could be expected from cosine dependence [Fig. 6, $1/\cos(\theta)$]. For example, near 50 eV, there is a 65% reduction in SEE yield for electrons incident at 0°,

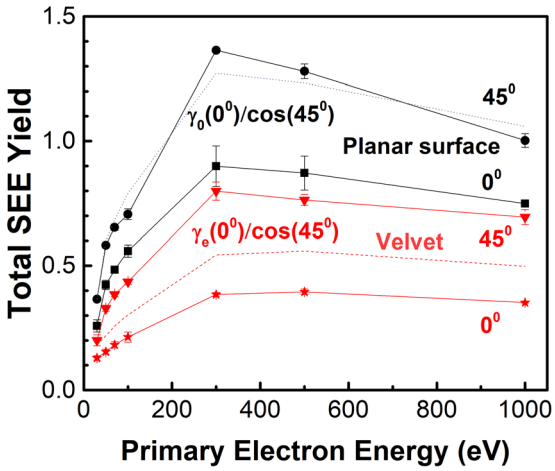

FIG. 6. The effect of the incidence angle of primary electrons on the total SEE yield measured for sample 2 (red symbols) (Table I) and for the graphite substrate without velvet (black symbols). Measurements are shown for normal incidence (pentagon-shape symbols) and the incidence angle of 45° (triangle-shape symbols). Measurements at 45° are compared to values calculated considering a $1/\cos(\theta)$ dependence (dashed curve). SEE yield for the graphite substrate at 0° (square-shape symbols), 45° (circle-shape symbols), and calculated values (dashed curve) are also plotted for comparison.

whereas there is a 43% reduction in SEE for primary electrons incident at 45°.

To evaluate this deviation from the cosine dependence, we assume that the probability density of the emission polar angles follows $\cos^{\alpha}\theta$ with a fitting parameter α.[22,23] From the results of Fig. 6, the α is almost twice larger than 1 (cosine law). It indicates that, with a larger value of α, the secondary electrons emitted from the bottom side become more focused in the normal direction. As a result, these electrons have higher probability to escape leading to a larger increase of the SEE yield with the incidence angle than that for the flat surface. This trend is in agreement with the modeling of the micro-porous surface.[23] The theoretical predictions of Ref. 17 demonstrate that the relative contributions of the flux of SEE electrons from the side walls of fibers is dominant at the incidence angle of 45°. This is because as the incidence angle increases, the primary electrons would hit the side walls of fibers rather than the bottom surface of the substrate. Any secondary electrons produced by these electrons will have a large probability to escape from the velvet. As a result, the total SEE yield increases. Note that even at the oblique incidence angle, the total SEE yield from the velvet samples remains below the SEE yield of the planar graphite samples at normal incidence.

IV. CONCLUSIONS

The results of measurements of the SEE yield from the carbon velvet samples with different packing densities and the velvet fiber lengths were presented. The total SEE yield from velvet can be up to 65% smaller than the SEE yield from the planar surface made of the same material. Velvet appears to be superior in terms of suppression of SEE as compared to foam[14] and other micro porous materials.[15] The measured SEE yield was compared with the theoretical predictions of Ref. 17. It appears that the model generally agrees with the results of the SEE measurements for samples with short fiber lengths (0.5 and 1.5 mm). However, there is a discrepancy between the measured and predicted SEE yield for samples with long fibers (3 mm). It is suggested that this discrepancy is due to the bending and tilting of long fibers. For such fibers, the primary electrons are at oblique incidences causing an increase in the total SEE yield from velvet samples. This deficiency of the realistic velvet samples may partially explain why the reduction of the SEE yield did not reach a theoretical >90% reduction of the yield as compared to the planar surface, which was predicted in Ref. 17. This result points to the importance of the determination of the actual packing density for samples with architectured surfaces. The lower SEE yield values calculated by Ref. 17 model compared with the experimentally measured values by electron gun may be partially explained by higher packing densities. The tilted and bent fibers occupy more of the total velvet surfaces compared to the vertically aligned fibers, and have been found to increase the actual packing density by up to 84% with respect to the design packing density. This is much higher than the packing density values used in Ref. 17 (>4%). The simulated SEE yield predictions reported in Ref. 17 use the packing densities below 4.0%, while the SEM micrograph analysis has revealed that the measured velvet samples each have average packing densities larger than 63%. It is possible that a packing density saturation exists above which the Ref. 17 model does not apply. A comparison of the theoretical predictions with the results of simulations can be strongly affected by the realistic features of the actual surface-architectured materials.

Finally, we also demonstrated the effect of the incident angle of the primary electrons on the SEE yield from the velvet samples. The observed deviation of the angular dependence of the SEE yield from the cosine law is explained due to the increased contribution of SEE from the fiber side wall to the total SEE yield at oblique incidence.

ACKNOWLEDGMENTS

The authors wish to thank Professor Sankha Banerjee of the California State University, Fresno for the fruitful discussions and Alex Merzhevskiy for the technical assistance. A.O. and Y.R. acknowledge the support of this work by U.S. DOE. C.J. acknowledges the support of his fellowship at PPPL by the National Natural Science Foundation of China (Grant Nos. 11505123, 11375126, and 11435009), a project funded by the China Postdoctoral Science Foundation.

[1]Y. Raitses, I. D. Kaganovich, A. Khrabrov, D. Sydorenko, N. J. Fisch, and A. Smolyakov, IEEE Trans. Plasma Sci. **39**, 995 (2011).
[2]S. Mazouffre, S. Tsikata, and J. Vaudolon, J. Appl. Phys. **116**, 243302 (2014).
[3]S. I. Krasheninnikov, A. Y. Pigarov, and W. Lee, Plasma Phys. Controlled Fusion **57**, 044009 (2015).
[4]J. P. Gunn, Plasma Phys. Controlled Fusion **54**, 085007 (2012).
[5]M. R. Baklanov, J. F. D. Marneffe, D. Shamiryan, A. M. Urbanowicz, H. Shi, and T. V. Rakhimova, J. Appl. Phys. **113**, 041101 (2013).
[6]R. Tschiersch, M. Bogaczyk, and H. E. Wagner, J. Phys. D: Appl. Phys. **47**, 365204 (2014).
[7]D. Sydorenko, I. Kaganovich, Y. Raitses, and A. Smolyakov, Phys. Rev. Lett. **103**, 145004 (2009).
[8]G. D. Hobbs and J. A. Wesson, Plasma Phys. **9**, 85 (1967).
[9]M. D. Campanell, A. V. Khrabrov, and I. D. Kaganovich, Phys. Rev. Lett. **108**, 255001 (2012).
[10]D. Ruzic, R. Moore, D. Manos, and S. Cohen, J. Vac. Sci. Technol. **20**, 1313 (1982).
[11]I. Montero, L. Aguilera, M. E. Dávila, V. C. Nistor, L. A. González, L. Galán, D. Raboso, and R. Ferritto, Appl. Surf. Sci. **291**, 74 (2014).
[12]L. Aguilera, I. Montero, M. E. Dávila, A. Ruiz, L. Galán, V. Nistor, D. Raboso, J. Palomares, and F. Soria, J. Phys. D: Appl. Phys. **46**, 165104 (2013).
[13]R. Cimino, M. R. Masullo, G. Bregliozzi, S. O'connor, S. Petracca, V. Baglin, A. Stabile, and A. Romano, in *Proceedings of IPAC2014, Dresden, Germany* (2014), pp. 2332–2334.
[14]M. Patino, Y. Raitses, and R. Wirz, Appl. Phys. Lett. **109**, 201602 (2016).
[15]M. Ye, Y. N. He, S. G. Hu, R. Wang, T. C. Hu, J. Yang, and W. Z. Cui, J. Appl. Phys. **113**, 074904 (2013).
[16]Y. Raitses, D. Staack, A. Dunaevsky, and N. J. Fisch, J. Appl. Phys. **99**, 36103 (2006).
[17]C. Swanson and I. D. Kaganovich, J. Appl. Phys. **120**, 213302 (2016).
[18]A. Dunaevsky, Y. Raitses, and N. J. Fisch, Phys. Plasmas **10**, 2574 (2003).
[19]M. I. Patino, Y. Raitses, B. E. Koel, and R. E. Wirz, J. Phys. D: Appl. Phys. **48**, 195204 (2015).
[20]R. A. Shatas, J. F. Marshall, and M. Pomerants, Phys. Rev. **102**, 682 (1956).
[21]H. Bruining, *Physics and Applications of Secondary Electron Emission* (McGraw-Hill, New York, 1954).
[22]M. A. Furman and M. T. F. Pivi, Phys. Rev. Accel. Beams **5**, 124404 (2002).
[23]M. Ye, D. Wang, and Y. He, J. Appl. Phys. **121**, 124901 (2017).